A Methodology For Optimal Designing Of Monitoring Sensor Networks For Tsunami Inversion

Joaquín Meza[1], Patricio A. Catalán[1,3,4], and Hiroaki Tsushima[2]

[1]Departamento de Obras Civiles, Universidad Técnica Federico Santa María, Valparaíso, Chile.
[2]Meteorological Research Institute, Japan Meteorological Agency, Tsukuba, Japan
[3]Centro de Investigación para la Gestión Integrada del Riesgo de Desastres (CIGIDEN), Santiago, Chile.
[4]Centro Científico Tecnológico de Valparaíso-CCTVal, Universidad Técnica Federico Santa María, Valparaíso, Chile.

Correspondence to: Joaquin Meza (joaquin.meza@usm.cl)

Abstract. A methodology to optimize the design of an offshore tsunami network array is presented, allowing determination of the placement of sensors to be used in an Early Tsunami Warning System framework. The method improves on previous sensor location methods by including multiple tsunami parameters as a measure of the predictive accuracy through a single cost function. The use of different tsunami parameters allows for a network which is less subject to bias found when using a single parameter. The resulting network performance was tested against a historical event, suggesting that having such a network in place could have provided meaningful information for the hazard assessment. The low number of sensors required may be useful in implementing such networks in places where funding of denser arrays might be of concern.

1 Introduction

Over the last decade, several tsunami events, such as those of Maule in 2010 and Tohoku in 2011, have further demonstrated the catastrophic and widespread potential for death and destruction inherent in tsunami waves and, at the same time, the need to improve the reliability of Tsunami Warning Systems (TWS). The 2010 Maule earthquake ($M_w = 8.8$) generated a tsunami that caused severe damage and loss of life in coastal communities (e.g. Fritz et al., 2011), and highlighted the consequences of an ineffective alert (Soulé, 2014). This event, and the improvements observed in the cases of other events, has reaffirmed the importance of improving timely evacuation warnings, which are considered to be one of the most effective ways to reduce the loss of human lives and damage to coastal communities (Okal, 2015).

Improving a TWS aims to the overarching goal of improving delivery of a timely and meaningful evaluation of the hazard to authorities, and through them to the population at large, with the main objective to trigger evacuation. While the role of education is usually considered the cornerstone for successful responses, the role of accurate information regarding the actual hazard is also relevant (Okal, 2015; Bernard and Titov, 2015). Over the years, improving the hazard assessment has followed different approaches. One common key aspect is maximizing the lead time of the warning relative to tsunami arrival to the area of interest.

For far field tsunami forecasting, where coastal tsunami impact can be evaluated well in advance of arrival time, the approach is to combine dense monitoring of the actual tsunami along its propagation path, and take advantage of this information to estimate the hazard. For instance, the United States has a worldwide network of offshore tsunami observatories, which are located near several subduction zones at distances equivalent to 30-60 minutes of tsunami wave travel time from expected tsunamigenic earthquake sources. This network was built by the Pacific Marine Environmental Laboratory of the National Oceanic and Atmospheric Administration, and it is termed the Deep-ocean Assessment and Reporting of Tsunamis (DART) system (e.g. Spillane et al., 2008; Percival et al., 2011). Ocean Bottom Pressure Sensors (OBPSs) record the tsunami and data are transmitted to data centers in real time by means of communication satellites (González et al., 2005). Data are then used as input to invert an estimate of a tsunami source (Percival et al., 2011), which allows forecasting a set of tsunami hazard products (Bernard and Titov, 2015).

For near field tsunamis forecasting, on the other hand, the short time interval between the tsunami generation and arrival may be insufficient to perform tsunami source evaluations and propagating forward the tsunami. As shown by Williamson and Newman (2018), in some places first arrivals can occur in as little as 5 min. For example, Aránguiz et al. (2016) reported arrivals in less than 8 min for the $M_w 8.4$ Illapel earthquake and tsunami, based on anecdotal evidence. Adding to this significant constraint, a relevant aspect of the problem is the finite time required to acquire data sufficient to allow for an inversion of the source. Owing to the significantly different propagation speeds between ocean surface and seismic waves, the preferred approach is to rely on seismic data alone. Although some seismic source solutions can be obtained in very short time, the inherent uncertainties can affect the accuracy of tsunami estimates which may limit its applicability (Cienfuegos et al., 2018). Moreover, the high computational cost of computing tsunami propagation and inundation, at least to date in operational systems, has prompted the use of table look-up procedures on data sets of scenarios calculated a priori stored in a database (e.g. Gica et al., 2008; Kamigaichi et al., 2009). This approach is used in countries such as Japan, Australia, and Indonesia, and recently, in Chile.

Nevertheless, it has been noted that including tsunami data in the inversion process usually leads to improved results in estimating the tsunami hazard (e.g. Behrens et al., 2010; Gusman and Tanioka, 2014; Gusman et al., 2014; Cienfuegos et al., 2018). Hence, it is highly desirable to incorporate tsunami data as early as possible in a TWS framework. These observations can be acquired from tide gage data (Satake, 1987; Satake and Kanamori, 1991), satellite altimetry (Arcas and Titov, 2006; Hirata et al., 2006), deep-ocean tsunameters (Titov, 2009; Percival et al., 2011) and cabled ocean bottom pressure sensors (OBPSs, Baba et al. (2004); Tsushima et al. (2009, 2012)). Among these, the use of coastal stations (tide gages) is typically not considered for early warning, owing to the nil lead time and possible influence of coastal bathymetry in the hydrodynamics, hence obfuscating the effect of the tsunami source. Hence, offshore tsunami data from tsunameters or OBPSs seem to be the most appropriate for TWS.

Williamson and Newman (2018) analyzed the possible coastal locations where sensors can provide a meaningful lead time, in a near field setting. These locations concentrate along narrow bands that run roughly parallel to subduction zones. In addition, one of the most important factors for tsunami forecasting based on offshore tsunami data is the array configuration of tsunami stations. The accuracy of tsunami source reconstruction strongly depends on the azimuthal coverage of recording stations with respect to the source area (e.g. Pires and Miranda, 2001; Piatanesi et al., 2001; Bernard et al., 2001). In other words, accuracy depends whether the sensors are located close to the main beam of tsunami energy. In addition, when an adequate amount of sensors surround the tsunami source area with substantial azimuth coverage, it is possible to determine with greater detail the tsunami source. Hence, a dense network of sensors might be required. To date, only four developed countries, the U.S., Japan, Canada and Oman, are able to maintain dense cabled sensor networks. A major handicap is the high cost of the sensors themselves and their installation, as well as their subsequent operation and maintenance. For instance, Japan has a few submarine cabled seafloor observatory networks (e.g. the S-net, DONET1 and DONET2 systems) that provide data in real time. A 1000 km cabled observatory with 164 bottom pressure sensors was installed at an estimated cost of US$ 500M (Bernard and Titov, 2015). This high cost may pose a significant hurdle for developing countries along subduction zones, such as Chile or other countries on the eastern Pacific seaboard, where the seismogenic zone is extensive. However, despite this potential economic hurdle, it is relevant to study whether less dense arrays could provide a working solution at lower cost.

The placement of tsunameters has been based on expert judgment which considered technical aspects such as variability and location of seismic sources (Schindelé et al., 2008), travel time (Schindelé et al., 2008; Omira et al., 2009; Williamson and Newman, 2018), financial (Araki et al., 2008), and legal aspects (Abe and Imamura, 2013), among others. Bernard et al. (2001) suggested that along-strike sensor spacing of about 175-700 km is required to characterize the main energy beam of $M_w \sim 8.0$ events with just three sensors. The actual spacing will depend on the allowed elapsed arrival time to the sensors. In order to improve the tsunami warning efficacy to design tsunamis observation networks, Schindelé et al. (2008); Omira et al. (2009) took into account the seismicity to identify possible sources, and designed the optimal placement of sensors using as target function the travel time and a set of delays. In particular, Schindelé et al. (2008) use 16, evenly spaced sources spanning a long stretch of coast of the Western Mediterranean basin, which are used to test the efficacy of a set of two predefined arrays. 13 tsunameters spaced about 50-90 km yield the best results. Omira et al. (2009) use just a single scenario for each of five tsunamigenic zones, but on a smaller domain, resulting in a array consisting of just three sensors. On the other hand, Spillane et al. (2008) carried out an optimization approach to place DART buoys in Aleutians and Alaska regions. Time detection was the main restriction to place tsunameters, where it was found that adding more than three sensors did not improve the results significantly. Mulia et al. (2017a) used a similar approach, but a dimensionality reduction approach was incorporated to initiate the optimization. Unlike the previous cases where the goal was to address performance for a wide range of sources, Mulia et al. (2017a) and Mulia et al. (2017b) aim at the best placing of sensors to characterize a large–magnitude, target scenario. Here, the focus is to capture with great detail the characteristics of non-uniform slip by maximizing the accuracy of inverting a set of stochastic scenarios on a predefined domain. Inverted slips are compared against each stochastic source, under the assumption that tsunami parameters will be well determined if the earthquake source is well retrieved. Hence, no evaluation of

the tsunamis are performed. An initial set of 30 sensors is obtained, which can be reduced to 23 sensors at specific locations after optimization. This highlights that in pursuing the detailed structure of slip, a large number of sensors is required. Finally, Saunders and Haase (2018) proposed an improvement in slip characterization for the Cascadia Subduction Zone testing five different, dense sensor arrays. To assess the quality of results, the root mean square, maximum fault slip, tsunami amplitude at the coast and percentage of coastline hit by the high amplitudes waves between recovered from inversion and input data were compared, which expands on the preferred use of travel times as assessment parameter.

In the perspective of cost-performance ratio, it might be of interest to establish the minimal number and location of sensors required to provide a reasonable estimation. This purpose cannot be reached without taking into consideration the azimuthal coverage and the time required for observation, which strongly depends on the spatial relationship between the tsunami source and the tsunameters (e.g. Bernard et al., 2001). Although it is true that for both tsunami warning and scientific purposes, more data is always desirable, the number of deployments can limited for economic and technical reasons. For developing countries, a solution balancing cost and precision might be more appealing.

Consequently, in the present work, a methodology for estimating the optimal placement of a small numbers of sensors is used and tested. To carry out an objective comparison, three different tsunami parameters are considered in unison to find the optimal configuration. The performance of the resulting network is evaluated by simulating its application to the tsunami of Pisagua 2014 (Catalán et al., 2015).

2 Methodology

The overall objective is to determine an optimal array configuration of offshore tsunami sensors for near-field tsunami forecasting, to be used as a data source for a tsunami inversion technique. In what follows, the analysis will focus in optimizing the forecast accuracy of relevant tsunami parameters, and leaving aside other possible considerations such as cost or technical constraints on sensor placement. The methodology assumes the sensor are capable of providing free surface data at sufficient temporal resolution, therefore it is considered independent of the type of sensor. The methodology is similar in scope to previous studies (e.g. Schindelé et al., 2008; Omira et al., 2009), but here other tsunami parameters are included in the assessment. The method builds on the premise that, in order to determine the tsunami source, an inversion procedure must be implemented. While an inversion algorithm can be subject to a wide range of errors and uncertainties on its own, for the purpose of the present work it is hypothesized that using a single inversion procedure will weigh equally those errors allowing comparison among different sensor configurations. Consequently, it is the procedure presented herein can be applied independently of the inversion method, and the nature of the sensors. Similarly, other sources of signal noise such as atmospheric variations, tides, etc. It is noted also that in actual operational conditions, incoming data from sensors could need to be pre-processed as to improve the signal to noise ratio. For instance, Tsushima et al. (2012) use a 60 s moving average to process data from ocean

bottom pressure sensors. Moreover, in some cases, the quality of the data could be dependent on distance to the source. For the present case, these effects are not considered and it is assumed the inversion process is free of its influence. In addition, it is expected that the resulting network could be used for a range of source locations, hence spatial dependencies are not considered and weighed equally.

In this case, the "tsunami Forecasting based on Inversion for initial sea-Surface Height" (tFISH) algorithm is used (see Tsushima et al., 2009, for details). To carry out the inversion analysis, offshore tsunami waveform data are inverted (in real time in an operational setting) to estimate the initial distribution of the sea surface displacement. Coastal tsunami waveforms are then synthesized by linearly combining pre-computed tsunami Green's functions weighted by the resulting initial distribution. The method allows for considering the coseismic displacement in the inversion procedure, thereby allowing to place sensors in the seismogenic zone. More details about tFISH can be seen in Tsushima et al. (2009, 2012).

The use of Green's functions is preferred over directly modeling individual events to target sensor locations (e.g. Schindelé et al., 2008) because it allows for testing and comparing a large number of sensor configurations at low computational cost, provided a quantitative parameter or cost function is defined for the comparison. To compute the Green's Function for each subfault patch, a numerical scheme of the linear long-wave equations is used to propagate each tsunami elemental source to a set of predefined forecast points. The initial sea surface model for each Green's function is represented by a Gaussian function. Overlapping Green's functions are considered to express smooth variations of sea-surface displacement with a finite number of discrete elements (Aida, 1972). For the purposes of the present work, a set of nearly 1000 Green's functions is considered. Each of them is of dimensions of 700 x 700 arc seconds, with its centers spaced 0.15 arc-deg. They cover an area spanning about $7^\circ \times 3^\circ$ (latitude and longitude), consistent with the so called Northern Chile Gap (Comte and Pardo, 1991; Metois et al., 2013). In what follows, although an inversion process can benefit by other data sources such as Deep ocean Assessment and Reporting of Tsunamis (DART) buoys, these are not considered in the analysis under the premise that the area of interest is developing a completely new system. On the other hand, for the particular case of Chile, the location of the existing DART buoys in the area of interest is such that requires longer observation times than the ones studied here (Williamson and Newman, 2018).

Tsunami free surface time series, $\eta(t)$, are computed at a set of offshore and coastal observation points for a prescribed duration of the event, T. The offshore observation points are considered possible locations of a single observing station or sensor, and a subset of sensors is termed a sensor array. Typically, these are located at absolute depths such than nonlinear effects can be neglected thereby linear superposition of tsunami time series can be performed with minimal errors. The coastal observation points correspond to tide gages, which are used to evaluate the predictive performance at the coast.

The overall procedure considers that given a source event, and for a given observation array, it is possible to estimate an inverted tsunami source solution. This solution is then propagated to the coastal points, where a set of relevant parameters are assessed to evaluate the quality of the solution by comparing it against a target scenario calculated independently. To this end,

the error in three tsunami parameters is estimated. As others (e.g. Schindelé et al., 2008; Omira et al., 2009), tsunami arrival time is considered a key parameter, as it is essential in a TWS framework to provide a timely hazard assessment.

The definition of arrival time is relatively loose and could refer to different stages of the tsunami, such as the first exceedance of a threshold, the first local crest, first initial trough of N-waves, and others (e.g. Hayashi et al., 2011). Here, two different definitions are considered in order to make the analysis more robust. The first definition defines the time T_1 at which the tsunami exceeds a certain threshold

$$T_1(\eta) = \min(t \in (0,T) \mid \eta(t) > \epsilon). \tag{1}$$

This arrival time definition is also used by the German-Indonesian Tsunami Early Warning System (GITEWS) (Rakowsky et al., 2013). However, considering that in some cases, the tsunami time series might not exceed the threshold, a second arrival time is defined as the time when a proxy for the slope of the free surface exceeds a certain threshold

$$T_2(\eta) = \min\left(t \in (0,T) \mid \frac{\partial \eta}{\partial t} > \delta\right). \tag{2}$$

In this case, the idea is to establish a measure of the rate of change of the tsunami signal as an early proxy for the first local maximum. In doing this, it is assumed that the actual free surface slope is proportional to the rate of change as per the long wave approximation

$$\frac{\partial \eta}{\partial x} \propto \frac{\partial \eta}{\partial t}. \tag{3}$$

However, the accuracy in predicting the free surface time series is also relevant for a TWS. A key parameter is the maximum tsunami amplitude (here denoted as H), which is the parameter used to categorize the hazard in most existing TWSs. The maximum tsunami amplitude is estimated as

$$H = \max(\eta(t) - \eta(0) \mid t \in (0,T)). \tag{4}$$

It is of note that neither arrival time nor the maximum tsunami amplitude consider the accuracy in retrieving the shape of the waveform. Hence, the skill estimator is also introduced (S_k), as this index is commonly used to evaluate numerical performance of a model (e.g. Hampson et al., 2011)

$$S_k = \sqrt{\frac{\frac{1}{n}\sum_{i=1}^{n}\left(\eta_{\text{for}} - \eta_{obs}\right)^2}{\frac{1}{n}\sum_{i=1}^{n}\left(\eta_{obs}\right)^2}}, \tag{5}$$

where η_{for} and η_{obs} are the time series forecasted from the inverted source, and the target or observed source at a location of interest, respectively. n represents the number of time steps of the time series.

In assessing the accuracy, the error between observed and forecasted quantities is estimated for arrival times and maximum tsunami amplitudes. However, one possible difficulty in establishing a standard metric is that each of these parameters has its own scale with significantly different ranges of values. For example, while a error in arrival time of a a few minutes can be considered reasonable (for instance, less than five), a variation in height of more than one meter can signify a large error. To provide a common comparison basis for all possible sensor configurations, each parameter error is adimensionalized by dividing by the reference provided by the observed dataset. In addition, it is possible that one parameter having a large error could bias the combined assessment to be implemented. Therefore, the error estimated is capped under the consideration that errors larger the observed value will be treated as equally significant. This is is implemented as follows

$$\Delta T_m = \min\left\{\left|\frac{T_m(\eta_{obs}) - T_m(\eta_{for})}{T_m(\eta_{obs})}\right|;1\right\}, \tag{6}$$

$$\Delta H = \min\left\{\left|\frac{H(\eta_{obs}) - H(\eta_{for})}{H(\eta_{obs}) - \eta(0)}\right|;1\right\}, \tag{7}$$

$$S_k = \min\left\{S_k;1\right\}. \tag{8}$$

where $m = 1, 2$ applies for the different time travel parameters. In the case of the skill, $S_k = 1$ indicates that the magnitude of the error is comparable or greater than the observed values. Zero values mean a perfect fit on the indicator. In addition, whether each quantity is under or overestimated is not considered relevant and absolute values are used.

While it is possible to analyze each of these metrics independently, it is also desirable to identify the sensor configuration that yields the minimum combined error. However, it might be relevant for the user to give preference to one of the metrics above the others. Hence, to combine all estimators into a single quantitative estimate, a forecasting accuracy function is introduced

$$F_{i,j}(\Delta T, \Delta H, S_k) = \alpha \Delta T_{i,j} + \beta \Delta H_{i,j} + \gamma S_k i, j, \tag{9}$$

which allows quantifying the total error of the estimation at the forecasting point j given an offshore array i. α, β and γ are weights that allow for user-defined tuning of the relative importance of each parameter. The sum of the weights should add to one, as to preserve the comparison basis. As a first estimation, $\alpha = 0.40, \beta = 0.40$ and $\gamma = 0.20$ are considered, owing to the larger weight attributed to arrival time in previous research. Moreover, as to couple both definitions of arrival times, the error

estimator associated to this parameter was considered as the average of each percentage error, $\Delta T = 0.5(\Delta T_1 + \Delta T_2)$. In this way, it is possible to quantitatively compare the performance of all sensor arrays at any given forecast point. By introducing the saturation value, errors ΔT_m or ΔH exceeding 100% are not penalized in excess and do not bias the overall error, allowing highlighting the effect of the other parameters in the comparison.

5

However, it is of interest to test global accuracy of the method at several forecast points simultaneously. For instance, to evaluate how a given network configuration improves the predictive capability at several coastal sites. The overall performance is computed by simply adding up the individual results at forecast points of interest, given a sensor array i

$$EG_i = \frac{1}{N}\sum_{j=1}^{N} F_{i,j}(\Delta T, \Delta H, S_k), \tag{10}$$

10 where N is the number of forecast points. Upon calculating the global error by means of Eq. 10 considering all possible offshore arrays, the candidate array is selected as that featuring the minimal global error $(\min(GE_i))$. As in the case of the Eq. 9, it is possible for Eq. 10 to be biased by a few forecast points. To this end, it is imposed that each forecasting point j of the array should have an accuracy function value smaller than a certain threshold ($F_{i,j}(\Delta T, \Delta H, S_k) < \mu, \quad \forall j$). This is equivalent to ensuring a minimal forecast capacity on each forecasting point j.

15

Regarding the construction of a sensor array, prior research indicates that two to four observation stations are capable of constraining the source parameters quite well if the stations are optimally located relative to the main tsunami energy beam, and adding more data does not significantly improve the inversion results (e.g. Percival et al., 2011; An, 2015). On the other hand, the relative distance of the sensors will depend on the time allowed to record the tsunami (e.g. Bernard et al., 2001).
20 Hence, given an earthquake, it is possible to define the area (henceforth termed listening area A_l) over which the tsunami waves have already propagated away from the source(e.g. Williamson and Newman, 2018). A minimum of two sensors must be considered inside this area. This equivalent to defining a data observation time, if the tsunami propagation speed is known. This time, termed T_0, represents the time the TWS allows for recording of the tsunami before performing an inversion.

25 To test the performance of the sensor arrays, a set of tsunami sources must be considered. While it is possible to test a large set of sources over a large domain as in Schindelé et al. (2008), here the focus is set on using sources located at the extreme of the area of interest, under the assumption that these will correspond to the worst scenario for the arrays owing to the decrease in sensitivity of detection as sensors are located further away of the main tsunami energy beam. Finally, once a sensor array has been defined, the candidate network is tested using other locations for synthetics sources and past events.

3 Data and Sensor Array Design

For the purpose of testing the possible sensor arrays, two tsunamigenic earthquakes, with seismic moments (M_w) 8.3 and 8.5 respectively, are considered as scenarios. These were determined by Cienfuegos et al. (2014) as representative events for the Northern Chile Gap. These are located just in front of Arica, near the Chile-Perú border, and just north of Peninsula Mejillones, as seen in Fig. 1. They also flank the rupture area of the 2014 Pisagua Earthquake. These scenarios were estimated from the interseismic coupling model of Chlieh et al. (2011), information on interseismic slip rates and convergence. The choice of the scenarios is based on the assumption that these constitute the worst case for performing an inversion. Hence, the optimal array should be capable of detecting each scenario and others located in between them.

A set of ~ 1000 unit tsunami sources were distributed uniformly over an area spanning 160 $\times$ 680 km. Tsunamis were propagated using the tsunami model JAGURS (Baba et al., 2016) to eight coastal stations (coinciding with existing tide gages operated by the National Hydrographic and Oceanic Service of the Chilean Navy, SHOA, by its acronym in Spanish). A subset of these will constitute the forecast points where the accuracy functions $F_{i,j}$ are valuated. They are also propagated to an array of virtual observation points, each of which denote the possible location of a sensor. JAGURS is a numerical model for dispersive tsunami wave modeling. This is a parallel software which solves the nonlinear Boussinesq dispersive equations in spherical coordinates. To solve these equations, a leapfrog staggered-grid, finite-difference calculation scheme is used. Bathymetry considered GEBCO global data with spatial resolution of 30 arc seconds. All Green's functions were calculated in advance and stored in a database, from which appropriate functions were extracted and used for the inversion and forward calculation.

Although in operational conditions, the time series recorded at an actual sensor will also include other signals that could be considered as tsunami noise, these are not considered here under the premise that the approach used herein is to discriminate among sensor configurations, assuming the treatment of tsunami noise is equivalent across sensors. Similarly, it is noted that possible operational restrictions regarding sensor placement are obviated although they could be implemented straightforwardly.

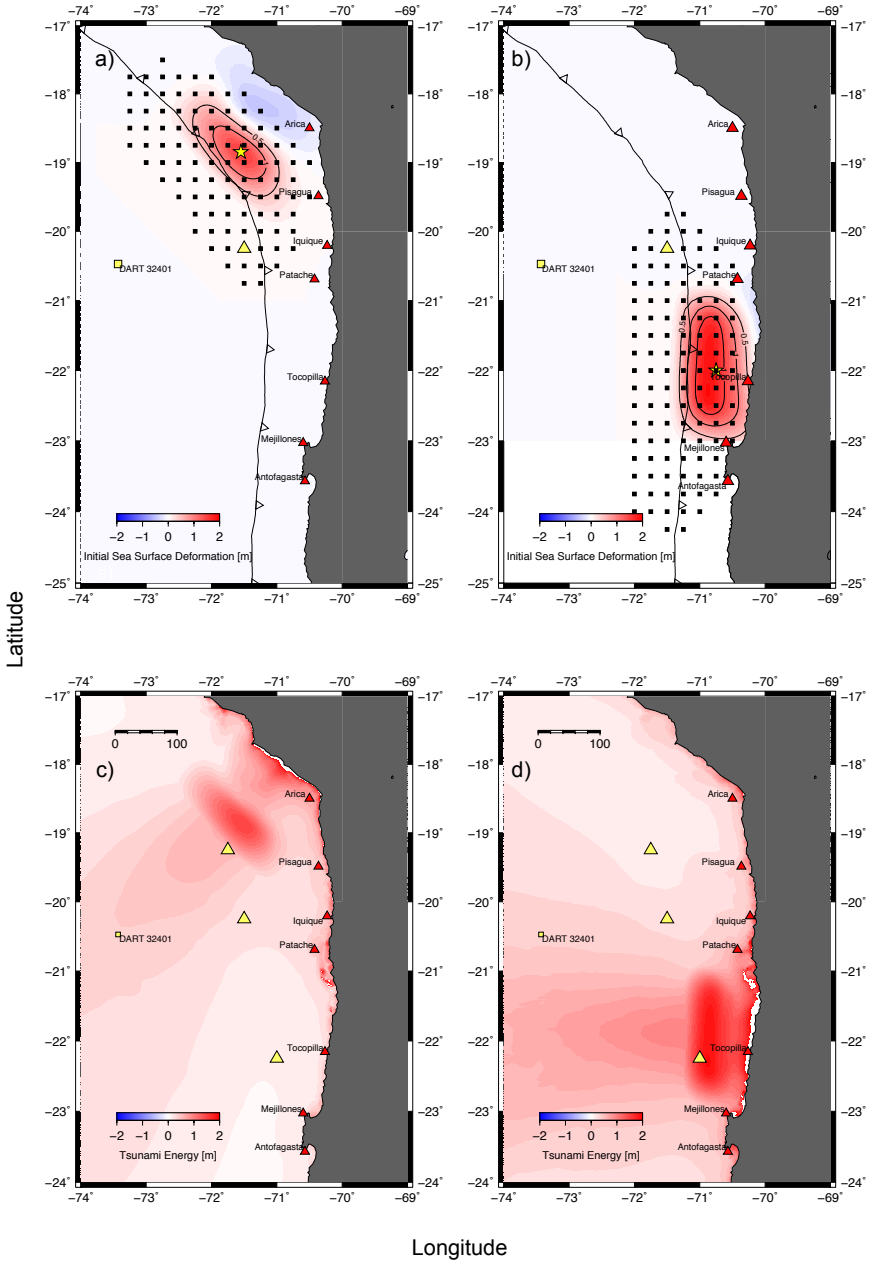

Figure 1. (a-b). Sea surface deformation for the scenarios considered. Stars indicate epicenters. Black squares show virtual observation points offshore, red triangles indicate the forecasting points, and the yellow triangle represents the fixed sensor. (a) shows a M_w 8.3 and (b) a M_w 8.5 scenarios, located in the northern and southern end of the the Northern Chile Gap, respectively.(c-d) are the corresponding maps of tsunami energy. In (c-d), the final sensor configuration is shown.

The relative position of each sensor to the tsunami scenarios, determine the tsunami arrival time to the sensor but also the elapsed observation time of data usable for inversion. In existing inversion procedures, each sensor uses a different observation time, sufficient to gather at least a quarter of the initial tsunami waveform. Here, the observation time T_0 is defined as to determine an area such as any sensor located inside of this area could record at least half a tsunami wavelength ($0 < t < T_0$). This defines the listening area, A_l. It is noted that the observation time is also restricted by the tsunami arrival to the coast, in order to provide sufficient lead time for an eventual warning. As a starting point, T_0=10 min is used, consistent with the observed tsunami arrival for 2014 Pisagua tsunami (Catalán et al., 2015).

Each of the tsunami scenarios is propagated to determine its propagation time and estimate the listening area. Considering the time restriction imposed, there is relatively small region where the listening area A_l of both scenarios overlap. Hence, it is possible to place a sensor that would serve both the northern and southern sections, located in the outer rise offshore of Iquique (see yellow triangle in Fig. 1). To find the location of the other sensors, the listening area for each scenario is discretized regularly every 0.25 arc degrees ($\sim$ 30 km) in both latitude and longitude, which is significantly less than the tsunami wavelength in the area. Each node is considered a possible sensor location. In addition, the nodes are to be located at depths large enough for tsunami nonlinear effects to be considered negligible, thereby ensuring consistency with the assumption by the inversion algorithm. As a consequence, 99 and 113 possible nodes are defined in the northern and southern parts, respectively, denoted as black squares in Fig. 1. The difference in the number of nodes is due to the differences in the source dimensions, and in tsunami celerity arising from the bathymetry, which in unison determine different listening areas. A sensor array was defined by the pairing of the common sensor and each of the possible nodes.

To carry out the analysis, each scenario is propagated forward to all forecast points (FPs), using the Nonlinear Shallow Water Equations as implemented in the model COMCOT. The time series at nodes in deep water are considered as target (observed) time series to be used in the inversion process, whereas the use of coastal forecast points is aimed at establishing the quality of the assessment (see below). The use of a different tsunami model in propagating the signal and in preparing the database of Green's functions allows for differences in the target tsunami time series to those of the database, to reduce possible overfitting in the inversion. No other source of variability, such as noise, is considered. It is also assumed that tsunami-tide interactions do not play a significant role in this area.

For each of the 212 sensor arrays (99 and 113, for each scenario), these observed tsunami time series are used to invert the tsunami source. Once a source is determined, the linear combinations of the Green's functions consistent with the source weights are used to estimate the forecast time series in the coastal points. It is of note that the use of linear superposition at shallow coastal points might be subject to inaccuracies arising from neglecting nonlinear interactions, and other process such as bathymetry–induced effects such as resonance. However, it is expected that omitting these process will affect the accuracy but not does limit discriminating among sensor configurations. Moreover, coastal points are located at 200 m. depths to reduce the effect of nonlinearity.

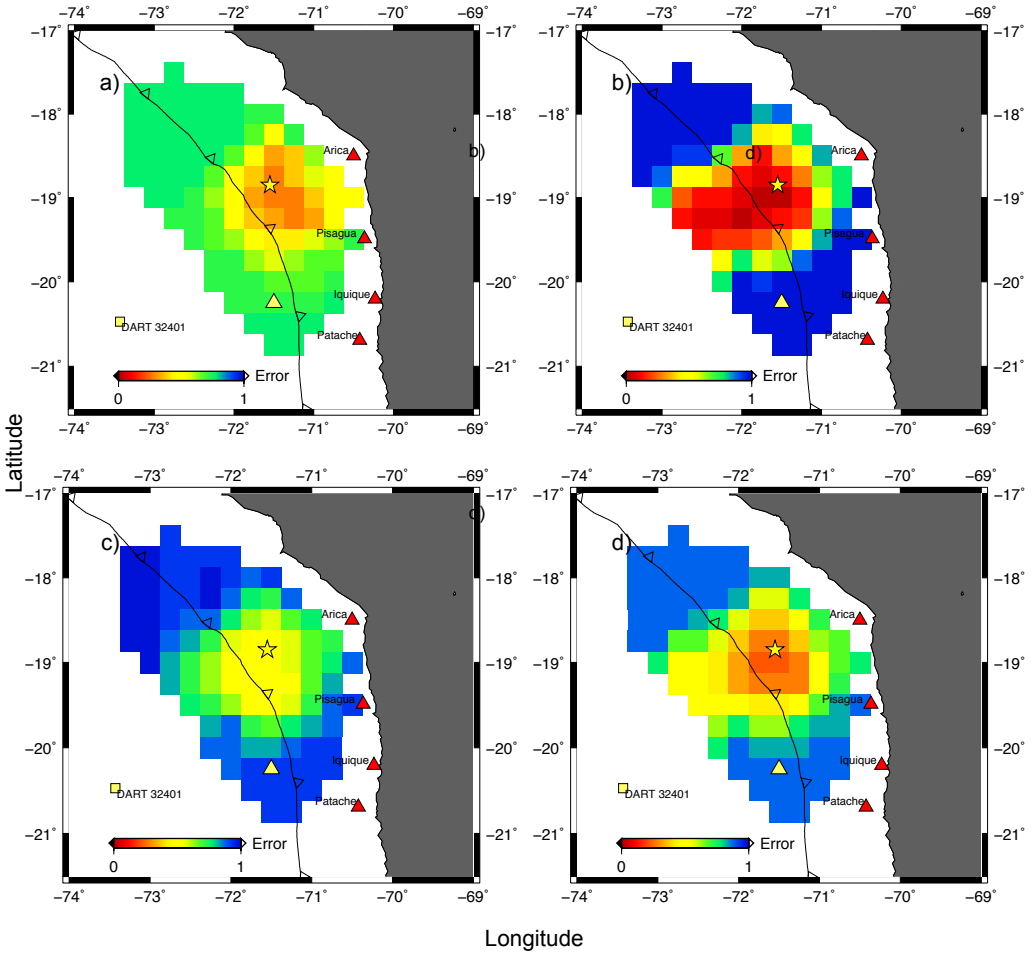

Figure 2. Spatial distribution of the individual error estimates, as a function of sensor arrays in the northern section. (a) ΔT (Eq. 6); (b) ΔH (Eq. 7); (c) S_k (Eq. 8); and (d) Total forecasting accuracy function, $F_{i,j}$ (Eq. 9) estimated using as reference the coastal forecast point in Arica. Star indicates the scenario epicenter, the thin black line is the location of the trench, the yellow triangle denotes the location of the fixed sensor, and each grid point in the color map corresponds to a movable sensor.

Consequently, the observed (from the full tsunami simulations using COMCOT) and the forecasted (from the linear combination using inverted source solutions) are compared to assess the accuracy of the solution. To this end, individual and aggregate error estimates (Eqs. 6-10) are calculated .

4 Results

Coastal points are located in front of the main cities where a tide gage is present, at 200 meters depth, consistent with the linear propagation used by tFISH. Waveforms obtained through inversion were compared with observed waveforms by means of the Eq. 9.

In Figs. 2 and 3, the accuracy of the estimation is presented as a space map of the value of each of the error estimates defined by Eqs.6 - 9, presented as a colorscale. Each grid point corresponds to the location of the second sensor of the array. Smaller values (red colors) indicate better accuracy. Results are presented when the evaluation is carried out using as a observed time series that of a coastal forecast point j at Arica and Patache, respectively.

The errors in arrival time, ΔT, (Fig. 2a and 3a), show better results when the sensors are close to the forecast point. This could be due to a better correspondence in arrival time between offshore and coastal waters. Arica and Patache show a distinct behavior, where Arica is more sensitive to the sensor location, with an error of $\sim 35\%$ on average, and accuracy reaching saturation at some locations (errors equal or greater than 100%). Patache shows less sensitivity and a better accuracy overall, partly because it benefits from the fixed sensor being located in front of it, making the results less sensitive to the placement of the secondary sensor.

The error in amplitude, ΔH is shown in Fig. 2b and 3b). Unlike the case of the arrival time, the performance at Arica and Patache are similar, suggesting that the movable sensor is more relevant in determining the tsunami amplitude, allowing for a better estimation. This pattern is related to the directivity of the tsunami energy radiation. When the tsunami source has an aspect ratio (length to width) greater than one, most of the tsunami energy is radiated perpendicular to the major axis of the source (Kajiura, 1970, 1972). Consequently, errors smaller than 17% are found in some cases where the sensor is located close to the main energy beam. In contrast, when the sensor is located parallel to the major axis, where weaker amplitudes are radiated, tsunami wavefronts used as input do not contain information about the maximum tsunami energy so that the initial sea surface is underestimated and leads also to underestimation of the amplitude at FPs. When sensors are located outside the main energy beam, accuracy decreases rapidly down to the saturation limit. The location of the fixed sensor does not allow for improved inversions, explaining the similar performance at both sites. The difference in performance of the amplitude error and the travel time highlights the need of including the amplitude as a relevant tsunami parameter.

Similar conclusions are obtained from the skill indicator, where higher forecasting accuracy is obtained for sensor arrays with at least one sensor located in the main energy beam. The combination of these individual errors in the forecasting accuracy function, $F_{i,j}$ follows the same trend (panels d, in Fig. 2-3). The minimum global error is found in the area opposite to Arica, and is influenced by the amplitude error but aggregates the structure of the error in arrival time. On the other hand, in Patache, the global error distribution shows less contrast between locations than in Arica. These results reinforce the idea that a single

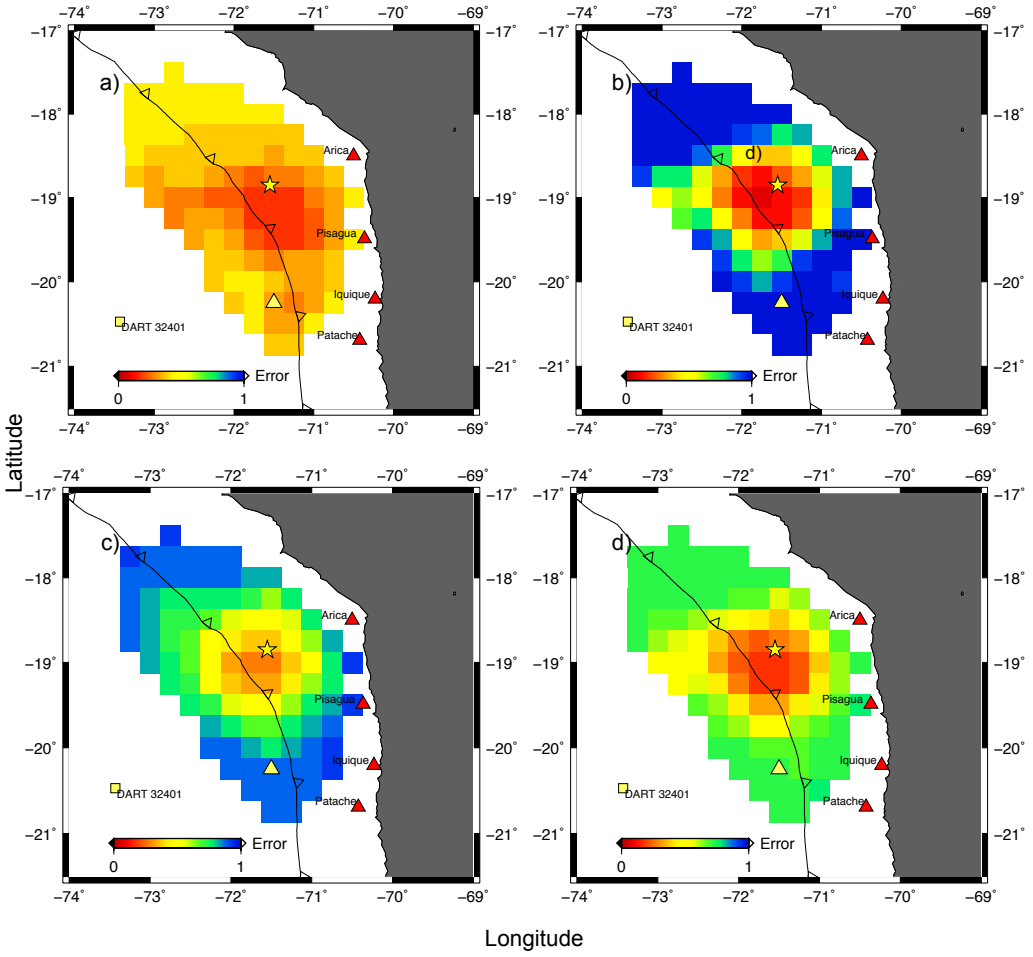

Figure 3. Same key as Fig. 2., using como reference the coastal forecast point at Patache.

error estimate such as arrival time is not sufficient to identify the best placement, but it also shows that using a single forecast point as a reference can be affected by local dependencies. It is important to note there is a smooth transition from lesser quality results (blue colors) to good quality results (red colors) for all estimators, which means that the spatial discretization used in sensor placement suffices to capture the error dependencies.

The aggregate of the forecasts at coastal points is estimated using Eq. 10, considering four coastal points for each scenario (N=4 in Eq. 10), namely Arica, Pisagua, Iquique and Patache, for the northern scenarios; and Patache, Tocopilla, Mejillones and Antofagasta for the southern scenario. The choice is due to their proximity to the source in each event and their importance

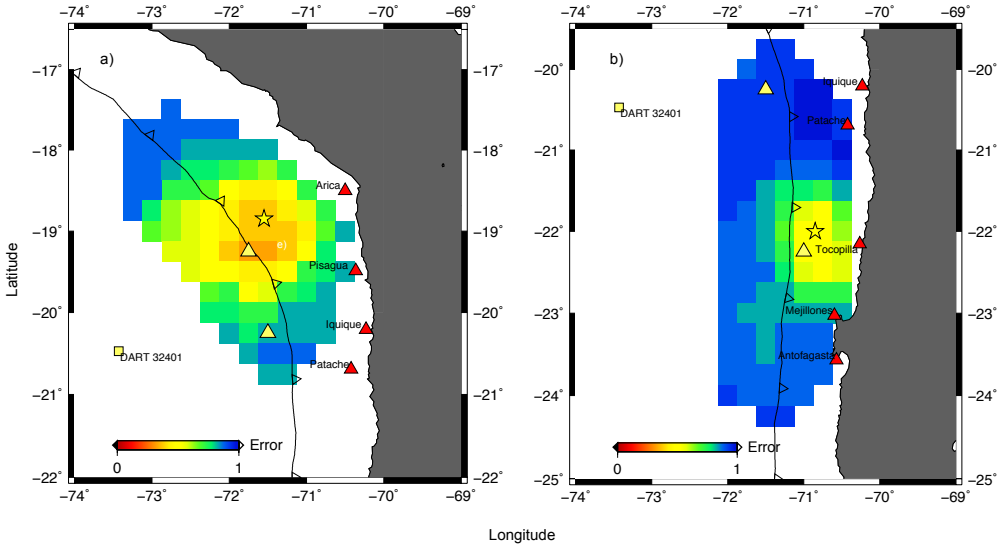

Figure 4. Space maps of global error, EG_i. Star indicates scenario epicenters, and yellow triangles show selected sensor array. (a) EG_i for the northern scenario, estimated using Arica, Pisagua, Iquique and Patache. (b) EG_i for the southern scenario, estimated using Patache, Tocopilla, Mejillones and Antofagasta.

in the north of Chile. Fig. 4 shows the global error for both events. As before, the spatial maps show a slight concentration of improved accuracy near the epicenter of earthquakes, but the variability is reduced owing to the averaging effect of considering several forecast coastal points in unison in the evaluation. Despite this, it is still possible to identify locations where a sensor could be deployed that yield the best overall performance. Therefore, the final array configuration is determined by identifying the configuration with minimum global error EG_i and that the total error for each coastal forecast point, $F_{i,j}$ is less than $\mu = 0.55$, to ensure a good quality at each FP. The selected coordinates of the sensor array are shown in Table 1 for reference.

Table 1. Sensor array configuration proposed.

Name	Latitude	Longitude
North	19.25° S	71.75° W
Fixed	20.25° S	71.50° W
South	22.25° S	71.00° W

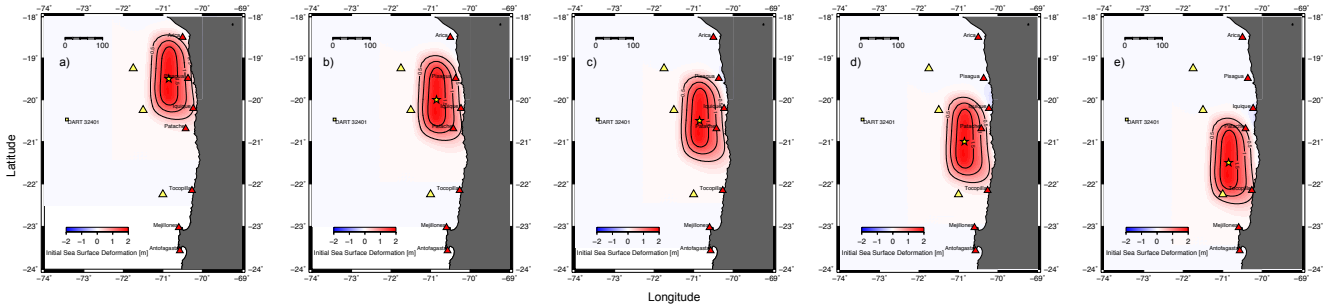

Figure 5. Initial sea-surface displacements used in evaluating the chosen sensor array. Red an yellow triangles indicate the forecasting points and sensors respectively. Epicenter are located at latitude (a) -19.5°, (b) -20.0°, (c)-20.5°, (d)-21.0 °; (e)-21.5°

5 Discussion

The methodology presented allows for an objective comparison of several array configurations, by using a set of relevant tsunami parameters. On the other hand, the method was tested by defining a minimum of two sensors to form a sensor array, under the premise that this represents the least expensive implementation. Testing for arrays comprising a larger number of sensors, and/or tsunami parameters, is straightforward and are not considered further in this work.

In addition, it is possible that for actual implementations, the selection of a sensor may provide additional restrictions. For example, the ability to transmit data in real time constraining to line-of-sight placement, or communications coverage; or deployment away from the trench to reduce the effect of seismic noise and coseismic signals, among many possible restrictions. Such restrictions were not considered herein as they can be sensor-specific, though they could be easily incorporated in the method by simply restricting locations where a sensor can be deployed.

The methodology proposed considered two characteristic scenarios located at the extremes of the area of interest. It is relevant to evaluate the capabilities of the proposed network in other cases to ensure that the proposed configurations do offer good performance not only for the target scenarios. To this end the southern event (M_w 8.5) was modeled in different epicentral locations along the subduction zone, every 0.5 arc degree along strike (see Fig 5). In addition, the listening time was changed (T_0=10, 15 and 20 min) to investigate the effect of record length on the forecast.

Fig. 6 shows the matrices of $F_{i,j}$ at each forecast point j as a function of the epicenter location, considering the final array configuration proposed, for different listening times, T_0. Regarding the latter, the aggregate error decreases as T_0 is increased, as expected, where aggregate errors can reach values as low as 15% when $T_0 = 20$ min (compare Fig. 6a and c). In the case

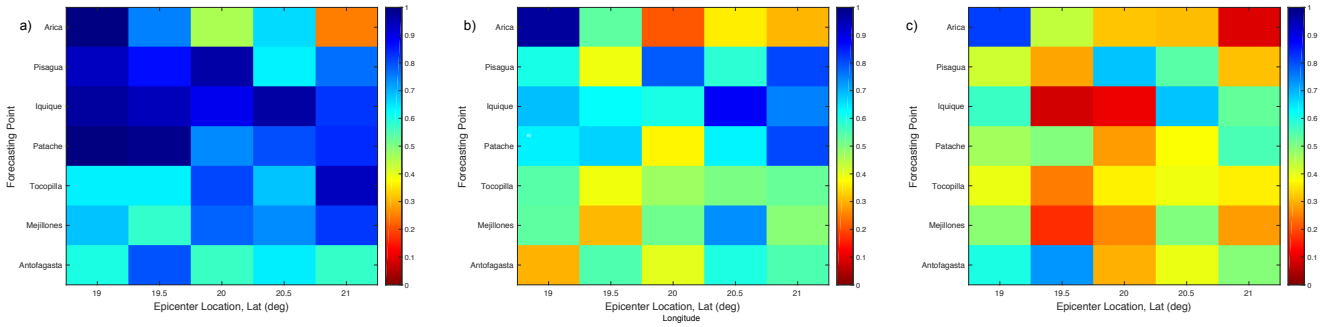

Figure 6. Forecast accuracy function $F_{i,j}$ as a function of reference forecast point j (vertical axis), considering different target scenario locations (horizontal axis) and listening time, T_0. (a) 10 min, (b) 15 min and (c) 20 min.

of Chile, where the seismic zone is located very close to the coast, this may prevent the use of this information as a trigger for early warning, but it could be considered in the later stages of the emergency cycle. For instance, this information can be used to refine initial hazard assessments derived by other means, such as the existing database of precomputed scenarios.

Regarding the sensor array performance for different scenarios, it is possible to observe a decrease in performance as the scenario is closer to the reference forecast point. This can be seen as a poor accuracy in the northern FPs (Arica to Iquique) for events with epicenters at latitudes -19.5° and -20° (see dark blue data in the upper left corner of Fig. 6a), and a worsening of the accuracy as the epicenters are located further south (see the evolution of the error for Tocopilla). This is due to the forecast points being placed close or inside the zone of the predicted coseismic deformation for the actual event, which prompts an early arrival in the observed signal. However, owing to the short listening time, the tsunami source solution results in a source of small spatial dimensions (see for example Fig. 7b, although for a different scenario). As result, the arrival time yields a large error. In the other cases, $F_{i,j}$ averages 40% which is considered a good performance for this observation time. As the observation time is increased, the error in the prediction drops significantly and values as low as $F_{i,j} \approx 20\%$ error can be obtained.

As an additional test for evaluating the potential performance of the sensor array, the tsunami of Pisagua on April 1st, 2014 ($M_W 8.1$) was used as source scenario. It is noted that this event has a smaller magnitude than the scenarios used in designing the network, and also that it has a non-uniform slip distribution, with two patches of slip. Synthetic tsunami waveforms at the location of the sensor array were obtained by a numerical simulation of the tsunami using the initial rupture model proposed by Hayes et al. (2014). As before, the accuracy of the assessment is evaluated using the coastal forecast points and different listening times, although in this case, the actual tide-gage records are considered. These were obtained from the IOC Sea Level

Monitoring Facility website.

Results are summarized in Table 2 and the initial surface solutions are shown in Fig. 7. It can be seen that within 10 min, the performance of the method is inadequate, with large errors and providing an inverted initial surface that only detects a localized source. As the observation time is increased, the errors decrease significantly, with the reconstructed sea surface condition now having an appropriate extension but a smaller peak displacement. The solution is improved for $T_0 = 20$ min, with errors as low as 8% (40% on average), and the solution includes traces of the secondary peak on the north west of the rupture. However, as mentioned before, such a sensor array would have only provided a timely assessment for locations outside the main rupture zone, since the observed tsunami arrival at the tide gages in Iquique and Pisagua was less than 15 min (An et al., 2014; Catalán et al., 2015).

Table 2. Summary of tsunami forecasting accuracy considering different data observation time for 2014 Pisagua event.

	Observation time		
Forecasting Point	10 [min]	15 [min]	20 [min]
Arica	0.66	1.00	1.00
Pisagua	0.83	0.90	0.70
Iquique	0.94	0.76	0.57
Patache	1.00	0.96	0.94
Tocopilla	0.83	0.77	0.79
Mejillones	0.59	0.55	0.54
Antofagasta	0.57	0.57	0.57

This suggests that the proposed network is capable of identifying smaller events with non-uniform slip reasonably well, in reasonable time. It is of note also that the location of this scenario does not coincide with either of the scenarios used to design the network. However, two of the sensors are located close but not directly into the main energy beam. When considered in unison, these two tests suggest that the sensor network considered would be appropriate for tsunamis generated by earthquakes of magnitude similar and larger than that of the initial target scenarios. It is possible, however, that a different network would be obtained if different target scenarios were used for the design. Nevertheless, the methodology allows for identifying a suitable sensor array. This stresses that one relevant step prior to the implementation of the methodology would be to determine these target scenarios by other means. In the present case, the choice was based on data available for the Northern Chile Gap.

On the other hand, the methodology expands on previous research by incorporating quantitatively different tsunami parameters in a cost function which can be minimized. However, the selection of the weights (α, β and γ) in the cost function $F_{i,j}$, Eq. 9, was arbitrary. To test the influence of these weights in the assessment, a sensitivity analysis was carried out. Each weight

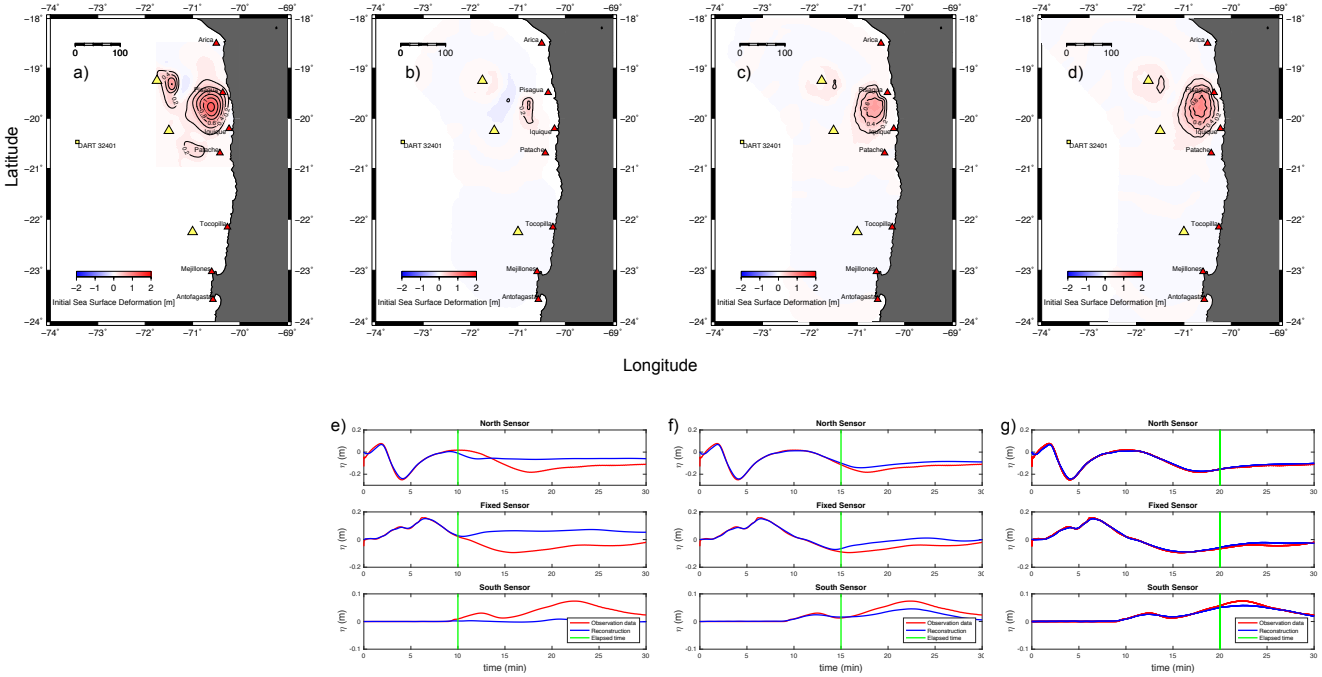

Figure 7. Initial sea surface displacement obtained from different listening times for the 2014 Pisagua tsunami. (a) Target result resulting from using the slip distribution of Hayes et al. (2014) as source scenario. (b) – (d) Distribution of the initial sea-surface displacement estimated by tsunami waveform inversion considering $T_0 = 10$, 15 and 20 min. (e) – (f) Comparison of observed (red lines) and calculated (blue lines) waveforms in the three sensors. Vertical green lines in (e), (f) and (g) indicate the listening time.

was modified by up to ± 0.1, with a 0.05 step. In addition, the case where only one parameter was used is also considered, yielding 23 weight combinations as shown in Table 3.

As a first step, it is analyzed whether modifying the weights induces a change in the selection of the sensor array. In Fig 8a-d, sample spatial maps of the global error EG are shown for some of the weight combinations (baseline combination, and combinations 10, 12 and 20, see Table 3 for details). It can be seen that although there is a variation of the value of the error, and also some variation of the spatial distribution of the magnitudes, the overall structure is consistent. The notable exception is combination 20, which only considers $\alpha = 1.0$, thus considering only the error in arrival times. Fig. 8e shows the value of the global error EG for each array configuration, as a function of the weight combination. For all combinations, the minimum error is obtained for the array 62, which is the one initially determined. This could be due to several factors. For instance, that the sensitivity range used in this test did not suffice to alter the result. However, even when only one parameter is considered,

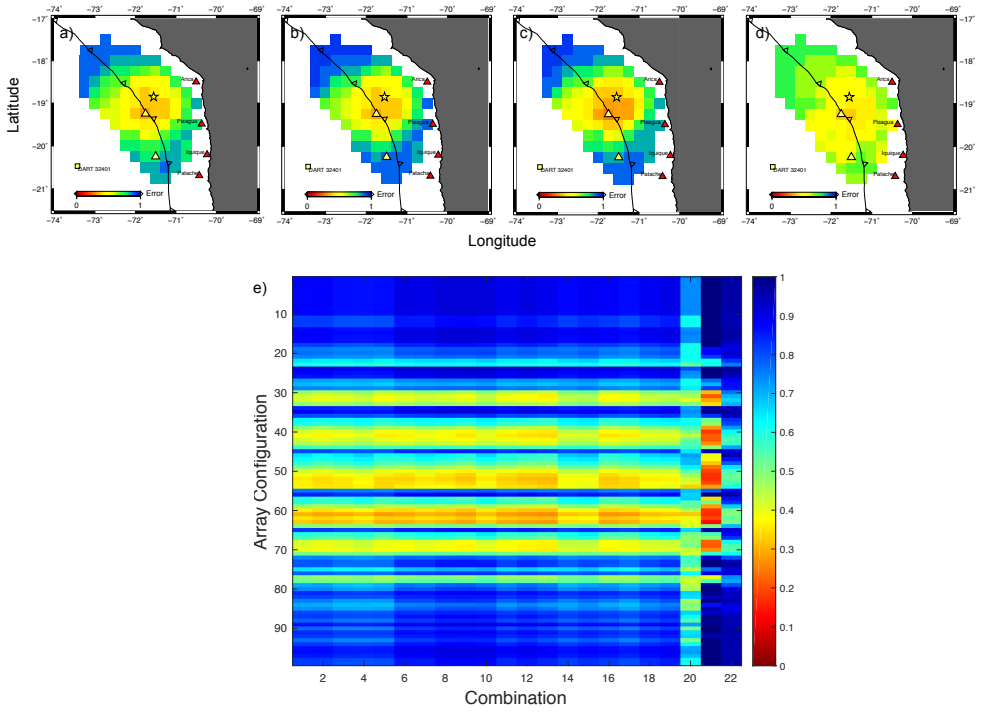

Figure 8. (a-d) Sample spatial maps of the global error, EG, as a function of the combination of weights. From left to right, combinations 1, 10, 12 and 20, respectively. (e) Matrix of the error EG for each sensor array as a function of the combination of weights. Array configurations are numbered in accordance to the grid location, from west to east, and then from north to south.

the solution remains unaltered. Consequently, it could be possible that the solution is controlled by only one parameter. For instance, the error in amplitude ΔH yields the minimum errors in several combinations (see red colors for combination 21 in Fig. 8e). However, there are some instances where it is the arrival time the parameter yielding the minimum error (see combination 20). Therefore, it is concluded that the use of a cost function combining both parameters maximizes the ability to capture well the overall structure of the tsunami signal. Moreover, the choice of weights proposed appears to be a good compromise among them.

Regarding the effect of the weighting on the accuracy assessment, it was also tested how much do the accuracy estimates for the Pisagua tsunami change with the different combinations of weights. The results are shown in Fig. 9, where it can be seen that in general, most forecast points have a relatively stable assessment, typically varying by less than 10% in the error estimate. However, the situation changes significantly if only one parameter is used. For instance, if only time is con-

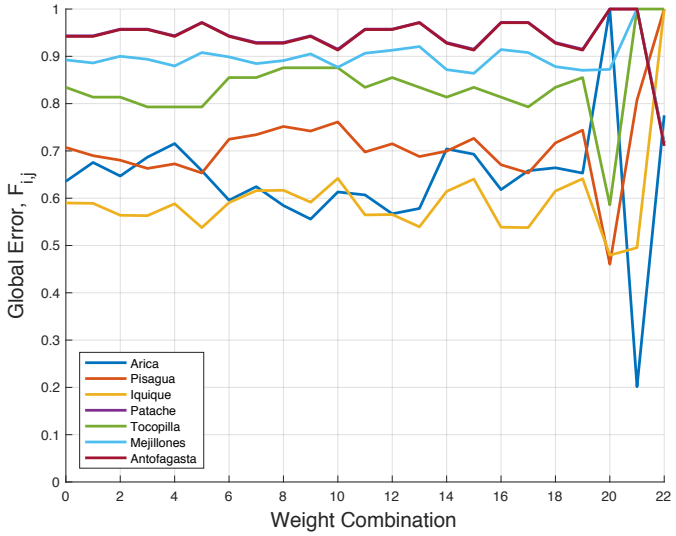

Figure 9. Forecasting accuracy by means of Equation 9 considering different weight combinations showed in the table 3 for the tsunami of Pisagua 2014.

sidered (combination 20), most forecast points worsen their assessment, as in Arica and Iquique. On the other hand, Patache and Antofagasta (which are overlapped since they have a similar, but not equal error, close to the saturation limit), shows a large drop in the error associated with the arrival time. The situation reverses when only the skill is considered (combination 22), when Arica and Iquique improve the estimation but Patache worsens significantly. Therefore, it is found that the use of multiple parameters is essential in producing a more complete estimation of the error for determining the optimal configuration.

The above results suggest the methodology is capable to deliver a working tsunami observation system comprised by just three sensors. Although the general rule that the spacing between sensor should be in the range $\sim$ 200-400 km (Bernard et al., 2001) is somewhat preserved, the spacing between sensors differs, between 110 and 225 km, approximately. This yields a less dense network as the one proposed by either Schindelé et al. (2008) and Omira et al. (2009). Moreover, the methodology

Table 3. Parameter space of weighting functions used.

Wei.	Combination																						
	0	1	2	3	4	5	6	7	8	9	10	11	12	13	14	15	16	17	18	19	20	21	22
α	0.4	0.45	0.45	0.5	0.5	0.5	0.35	0.35	0.3	0.3	0.3	0.4	0.35	0.4	0.45	0.4	0.45	0.5	0.4	0.35	1.0	0	0
β	0.4	0.35	0.4	0.35	0.3	0.4	0.45	0.4	0.45	0.5	0.4	0.45	0.5	0.5	0.3	0.3	0.45	0.4	0.35	0.35	0	1.0	0
γ	0.2	0.2	0.15	0.15	0.2	0.1	0.2	0.25	0.25	0.2	0.3	0.15	0.15	0.1	0.25	0.3	0.1	0.1	0.25	0.3	0	0	1.0

allows for the optimal placement of the sensors on this range of distances. On the other hand, the results show that, similarly to what is assumed by Gusman et al. (2014), the optimal placement corresponds to the area where the maximum displacement occurs. Considering the inherent uncertainty in predicting the slip distribution of the next earthquake, stochastic methods could be incorporated to this methodology to further refine the results. However, with the simulations performed here, it is possible to see that a small number of sensors can provide a baseline solution which would have been appropriate for an event such as that of Pisagua, 2014.

However, at least in a local context where arrival times are very short, it is also important to consider the actual benefit of incorporating such an evaluation in the context of early warning. The present results reaffirm that short observation times yield less accurate results. The balance between a quick assessment and accuracy must be considered in an Early TWS, and when the inherent uncertainties in inverting both earthquake and tsunami data are considered (Cienfuegos et al., 2018), it seems reasonable to propose that this information should be used for hazard assessment at later times of the emergency cycle, to refine quick hazard assessments estimated by other means, and not necessarily as the method for first evaluation.

6 Conclusions

This study presented a methodology, based on numerical simulations of near field tsunami forecasting, to determine an optimal array configuration of offshore tsunami sensors, with the goal of objectively determine the placement of the minimum set of sensors capable of providing an accurate estimation of the initial sea surface. To provide an objective basis for the comparison, three parameters are considered to assess the accuracy, thus expanding on previous methodologies that rely solely on arrival time. The joint use of the three estimators, arrival time ΔT, tsunami amplitude ΔH, and model skill S_k was robust when compared against a single parameter.

The methodology was tested in Northern Chile. Results showed that a configuration comprising a minimum of three sensors is capable of providing accurate estimations of the tsunami arrival time and peak amplitudes for the first wave. In this way, three sensors suffice to cover a 600 km stretch of coast when earthquakes in the M_w 8.0 range are considered.

Results show that there is a strong dependency between the location of the sensors and error estimators; arrival times are accurately predicted with sensors located opposite to the coastal point of interest. In addition, better results for tsunami amplitudes and skill are obtained when sensors are located inside the uplift or in front of it.

It should be noted that the methodology as proposed, assumes that incoming signals to the sensor network are accurate and free of noise. This assumption could not be applicable for certain type of sensors and some restrictions could be introduced in future work.

As a result, the methodology proposed shows promising potential to be used as an operational tool in defining the location of possible tsunameters, especially for sparse configurations in countries where the financial cost of implementing and maintaining dense networks could be an insurmountable hurdle.

Competing interests. The authors declare no competing interests/

Acknowledgements. This work was developed within the "Research Project on ENhancement of Technology To Develop Tsunami-Resilient Community", sponsored by Science and Technology Research Partnership for Sustainable Development, SATREPS Program by Japan Science and Technology (JST), the Japan International Cooperation Agency (JICA). PAC would also like to thank CONICYT through its grants FONDEF D11I1119 and IT15I10001, FONDAP 1511017 (CIGIDEN) and PIA-Basal FB0821 (CCTVal). Joaquin Meza has been supported by CONICYT through the MSc. Scholarship CONICYT-PCHA/Magister Nacional/2015–22150620 and by Dirección General de Investigación, Innovación y Postgrado, UTFSM.

References

Abe, I. and Imamura, F.: Problems and Effects af a Tsunami Inundation Forecast System During ahe 2011 Tohoku Earthquake, Journal of JSCE, 1, 516–520, https://doi.org/10.2208/journalofjsce.1.1_516, 2013.

Aida: Numerical Estimation of a Tsunami Source, Zisin (Journal of the Seismological Society of Japan. 2nd ser.), 25, 343–352, https://doi.org/10.4294/zisin1948.25.4_343, 1972.

An, C.: Inversion of tsunami waveforms and tsunami warning, Ph.D. thesis, Cornell University, 2015.

An, C., Sepúlveda, I., and Liu, P. L.-F.: Tsunami Source and Its Validation of the 2014 Iquique, Chile Earthquake, Geophysical Research Letters, 41, 3988–3994, https://doi.org/10.1002/2014GL060567, 2014.

Araki, E., Kawaguchi, K., Kaneko, S., and Kaneda, Y.: Design of deep ocean submarine cable observation network for earthquakes and tsunamis, in: OCEANS 2008 - MTS/IEEE Kobe Techno-Ocean, pp. 1–4, https://doi.org/10.1109/OCEANSKOBE.2008.4531071, 2008.

Aránguiz, R., González, G., González, J., Catalán, P. A., Cienfuegos, R., Yagi, Y., Okuwaki, R., Urra, L., Contreras, K., Del Rio, I., and Rojas, C.: The 16 September 2015 Chile Tsunami from the Post-Tsunami Survey and Numerical Modeling Perspectives, Pure and Applied Geophysics, 173, 333–348, https://doi.org/10.1007/s00024-015-1225-4, 2016.

Arcas, D. and Titov, V.: Sumatra tsunami: lessons from modeling, Surveys in Geophysics, 27, 679–705, https://doi.org/10.1007/s10712-006-9012-5, 2006.

Baba, T., Hirata, K., and Kaneda, Y.: Tsunami magnitudes determined from ocean-bottom pressure gauge data around Japan, Geophysical Research Letters, 31, https://doi.org/10.1029/2003GL019397, 2004.

Baba, T., Ando, K., Matsuoka, D., Hyodo, M., Hori, T., Takahashi, N., Obayashi, R., Imato, Y., Kitamura, D., Uehara, H., Kato, T., and Saka, R.: Large-scale, high-speed tsunami prediction for the Great Nankai Trough Earthquake on the K computer, The International Journal of High Performance Computing Applications, 30, 71–84, https://doi.org/10.1177/1094342015584090, 2016.

Behrens, J., Androsov, A., Babeyko, A. Y., Harig, S., Klaschka, F., and Mentrup, L.: A new multi-sensor approach to simulation assisted tsunami early warning, Natural Hazards and Earth System Sciences, 10, 1085–1100, https://doi.org/10.5194/nhess-10-1085-2010, https://www.nat-hazards-earth-syst-sci.net/10/1085/2010/, 2010.

Bernard, E. and Titov, V.: Evolution of tsunami warning systems and products, Philosophical Transactions of the Royal Society of London A: Mathematical, Physical and Engineering Sciences, 373, https://doi.org/10.1098/rsta.2014.0371, 2015.

Bernard, E. N., González, F. I., Meinig, C., and Milburn, H. B.: Early detection and real-time reporting of deep-ocean tsunamis, in: International Tsunami Symposium, Paper R-6, pp. 7–10, 2001.

Catalán, P. A., Aránguiz, R., González, G., Tomita, T., Cienfuegos, R., González, J., Shrivastava, M. N., Kumagai, K., Mokrani, C., Cortés, P., and Gubler, A.: The 1 April 2014 Pisagua tsunami: Observations and modeling, Geophysical Research Letters, 42, 2918–2925, https://doi.org/10.1002/2015GL063333, 2015GL063333, 2015.

Chlieh, M., Perfettini, H., Tavera, H., Avouac, J.-P., Remy, D., Nocquet, J.-M., Rolandone, F., Bondoux, F., Gabalda, G., and Bonvalot, S.: Interseismic coupling and seismic potential along the Central Andes subduction zone, Journal of Geophysical Research, 116, B12 405, https://doi.org/10.1029/2010JB008166, 2011.

Cienfuegos, R., Suarez, L., Aránguiz, R., Gonzalez, G., González-Carrasco, J. F., Catalan, P. A., Dominguez, J. C., and Tomita, T.: RE-ASSESSMENT OF TSUNAMI HAZARD IN THE CITY OF IQUIQUE, CHILE, AFTER THE PISAGUA EARTHQUAKE OF APRIL 2014 In the present contribution, we will reassess the tsunami hazard for the North of Chile taking into account the occurrence of the

recent events, focusing on the potential tsunami impact that a worse case scenario could produce in the city of Iquique., AGU Fall Meeting Abstracts, NH13A-3727, 2014.

Cienfuegos, R., Catalán, P. A., Urrutia, A., Benavente, R., Aránguiz, R., and González, G.: What can we do to forecast tsunami hazards in the near field given large epistemic uncertainty in rapid seismic source inversions?, Geophysical Research Letters, 45, 4944–4955, https://doi.org/10.1029/2018GL076998, 2018.

Comte, D. and Pardo, M.: Reappraisal of great historical earthquakes in the northern Chile and southern Peru seismic gaps, Natural Hazards, 4, 23–44, https://doi.org/10.1007/BF00126557, 1991.

Fritz, H., Petroff, C., Catalán, P. A., Cienfuegos, R., Winckler, P., Kalligeris, N., Weiss, R., Barrientos, S., Meneses, G., Valderas-Bermejo, C., Ebeling, C., Papadopoulos, A., Contreras, M., Almar, R., Dominguez, J., and Synolakis, C.: Field Survey of the 27 February 2010 Chile Tsunami, Pure and Applied Geophysics, 168, 1989–2010, https://doi.org/10.1007/s00024-011-0283-5, 10.1007/s00024-011-0283-5, 2011.

Gica, E., Spillane, M. C., Titov, V. V., Chamberlin, C. D., and Newman, J. C.: Development of the Forecast Propagation Database tor NOAAs Short-term Inundation Forecast For Tsunamis (SIFT), Tech. Rep. NOAA Technical Memorandum OAR PMEL-139, National Oceanic and Atmospheric Administration, 2008.

González, F. I., Bernard, E. N., Meinig, C., Eble, M. C., Mofjeld, H. O., and Stalin, S.: The NTHMP Tsunameter Network, Natural Hazards, 35, 25–39, https://doi.org/10.1007/s11069-004-2402-4, 2005.

Gusman, A. and Tanioka, Y.: W Phase Inversion and Tsunami Inundation Modeling for Tsunami Early Warning: Case Study for the 2011 Tohoku Event, Pure and Applied Geophysics, 171, 1409–1422, https://doi.org/10.1007/s00024-013-0680-z, 2014.

Gusman, A. R., Tanioka, Y., MacInnes, B. T., and Tsushima, H.: A methodology for near-field tsunami inundation forecasting: Application to the 2011 Tohoku tsunami, Journal of Geophysical Research: Solid Earth, 119, 8186–8206, https://doi.org/10.1002/2014JB010958, 2014JB010958, 2014.

Hampson, R., MacMahan, J., and Kirby, J. T.: A Low-Cost Hydrographic Kayak Surveying System, Journal of Coastal Research, 27, 600–603, https://doi.org/10.2112/JCOASTRES-D-09-00108.1, http://dx.doi.org/10.2112/JCOASTRES-D-09-00108.1, 2011.

Hayashi, Y., Tsushima, H., Hirata, K., Kimura, K., and Maeda, K.: Tsunami source area of the 2011 off the Pacific coast of Tohoku Earthquake determined from tsunami arrival times at offshore observation stations, Earth, Planets and Space, 63, 54, https://doi.org/10.5047/eps.2011.06.042, 2011.

Hayes, G. P., Herman, M. W., Barnhart, W. D., Furlong, K. P., Riquelme, S., Benz, H. M., Bergman, E., Barrientos, S., Earle, P. S., and Samsonov, S.: Continuing megathrust earthquake potential in Chile after the 2014 Iquique earthquake, Nature, 512, 295–298, https://doi.org/10.1038/nature13677, 2014.

Hirata, K., Satake, K., Tanioka, Y., Kuragano, T., Hasegawa, Y., Hayashi, Y., and Hamada, N.: The 2004 Indian Ocean tsunami: Tsunami source model from satellite altimetry, Earth, Planets and Space, 58, 195–201, https://doi.org/10.1186/BF03353378, 2006.

Kajiura, K.: Tsunami source, energy and the directivity of wave radiation., Bull. Earthq. Res. Inst., pp. 835–869, https://doi.org/10.1007/BF02109296, 1970.

Kajiura, K.: The directivity of energy radiation of the tsunami generated in the vicinity of a continental shelf, Journal of the Oceanographical Society of Japan, 28, 260–277, https://doi.org/10.1007/BF02109296, 1972.

Kamigaichi, O., Saito, M., Doi, K., Matsumori, T., Tsukada, S., Takeda, K., Shimoyama, T., Nakamura, K., Kiyomoto, M., and Watanabe, Y.: Earthquake Early Warning in Japan: Warning the General Public and Future Prospects, Seismological Research Letters, 80, 717, https://doi.org/10.1785/gssrl.80.5.717, 2009.

Metois, M., Socquet, A., Vigny, C., Carrizo, D., Peyrat, S., Delorme, A., Maureira, E., Valderas-Bermejo, M.-C., and Ortega, I.: Revisiting the North Chile seismic gap segmentation using GPS-derived interseismic coupling, Geophysical Journal International, 194, 1283–1294, https://doi.org/10.1093/gji/ggt183, 2013.

Mulia, I. E., Gusman, A. R., and Satake, K.: Optimal Design for Placements of Tsunami Observing Systems to Accurately Characterize the Inducing Earthquake, Geophysical Research Letters, 44, 12,106–12,115, https://doi.org/10.1002/2017GL075791, 2017a.

Mulia, I. E., Inazu, D., Waseda, T., and Gusman, A. R.: Preparing for the Future Nankai Trough Tsunami: A Data Assimilation and Inversion Analysis From Various Observational Systems, J. Geophys. Res. Oceans, 122, 7924–7937, https://doi.org/10.1002/2017JC012695, 2017b.

Okal, E. A.: The quest for wisdom: lessons from 17 tsunamis, 2004–2014, Philosophical Transactions of the Royal Society of London A: Mathematical, Physical and Engineering Sciences, 373, https://doi.org/10.1098/rsta.2014.0370, 2015.

Omira, R., Baptista, M. A., Matias, L., Miranda, J. M., Catita, C., Carrilho, F., and Toto, E.: Design of a Sea-level Tsunami Detection Network for the Gulf of Cadiz, Natural Hazards and Earth System Sciences, 9, 1327–1338, https://doi.org/10.5194/nhess-9-1327-2009, 2009.

Percival, D. B., Denbo, D. W., Eblé, M. C., Gica, E., Mofjeld, H. O., Spillane, M. C., Tang, L., and Titov, V. V.: Extraction of tsunami source coefficients via inversion of DART buoy data, Natural Hazards, 58, 567–590, https://doi.org/10.1007/s11069-010-9688-1, 2011.

Piatanesi, A., Tinti, S., and Pagnoni, G.: Tsunami waveform inversion by numerical finite-elements Green's functions, Natural Hazards and Earth System Sciences, 1, 187–194, https://doi.org/10.5194/nhess-1-187-2001, 2001.

Pires and Miranda: Tsunami waveform inversion by adjoint methods, Journal of Geophysical Research: Oceans, 106, 19 773–19 796, https://doi.org/10.1029/2000JC000334, 2001.

Rakowsky, N., Androsov, A., Fuchs, A., Harig, S., Immerz, A., Danilov, S., Hiller, W., and Schröter, J.: Operational tsunami modelling with TsunAWI â€“ recent developments and applications, Natural Hazards and Earth System Sciences, 13, 1629–1642, https://doi.org/10.5194/nhess-13-1629-2013, https://www.nat-hazards-earth-syst-sci.net/13/1629/2013/, 2013.

Satake, K.: Inversion Of Tsunami Waveforms For The Estimation Of A Fault Heterogeneity: Method And Numerical Experiments, Journal of Physics of the Earth, 35, 241–254, https://doi.org/10.4294/jpe1952.35.241, 1987.

Satake, K. and Kanamori, H.: Use of tsunami waveforms for earthquake source study, Natural Hazards, 4, 193–208, https://doi.org/10.1007/BF00162787, 1991.

Saunders and Haase: Augmenting onshore GNSS displacements with offshore observations to improve slip characterization for Cascadia subduction zone earthquakes, Geophysical Research Letters, 0, https://doi.org/10.1029/2018GL078233, https://agupubs.onlinelibrary.wiley.com/doi/abs/10.1029/2018GL078233, 2018.

Schindelé, F., Loevenbruck, A., and Hébert, H.: Strategy to design the sea-level monitoring networks for small tsunamigenic oceanic basins: the Western Mediterranean case, Natural Hazards and Earth System Sciences, 8, 1019–1027, https://doi.org/10.5194/nhess-8-1019-2008, 2008.

Soulé, B.: Post-crisis analysis of an ineffective tsunami alert: the 2010 earthquake in Maule, Chile, Disasters, 38, 375–397, https://doi.org/10.1111/disa.12045, 2014.

Spillane, M. C., Gica, E., Titov, V. V., and Mofjeld, H. O.: Tsunameter network design for the U.S. DART arrays in the Pacific and Atlantic Oceans, NOAA Technical Memorandum OAR PMEL-143, National Oceanic and Atmospheric Administration, 2008.

Titov, V.: Tsunami forecasting, in: , Chapter 12 in The Sea, Volume 15: Tsunamis, Harvard University Press, Cambridge, MA and London, England, 371–400., vol. 212, pp. 629 – 636, https://doi.org/10.1016/j.proeng.2018.01.081, 7th International Conference on Building Resilience: Using scientific knowledge to inform policy and practice in disaster risk reduction, 2009.

Tsushima, H., Hino, R., Fujimoto, H., Tanioka, Y., and Imamura, F.: Near-field tsunami forecasting from cabled ocean bottom pressure data, Journal of Geophysical Research, 114, B06 309, https://doi.org/10.1029/2008JB005988, 2009.

Tsushima, H., Hino, R., Tanioka, Y., Imamura, F., and Fujimoto, H.: Tsunami waveform inversion incorporating permanent seafloor deformation and its application to tsunami forecasting, Journal of Geophysical Research, 117, B03 311, https://doi.org/10.1029/2011JB008877, 2012.

Williamson, A. L. and Newman, A. V.: Suitability of Open-Ocean Instrumentation for Use in Near-Field Tsunami Early Warning Along Seismically Active Subduction Zones, Pure and Applied Geophysics, https://doi.org/10.1007/s00024-018-1898-6, 2018.